

Topological Invariant Tensor Renormalization Group Method for Edwards-Anderson Spin Glasses Model

Chuang Wang,^{1,2,*} Shao-Meng Qin,¹ and Hai-Jun Zhou¹

¹*State Key Laboratory of Statistical Physics, Institute of Theoretical Physics,
Chinese Academy of Sciences, Zhong-Guan-Cun East Road 55, Beijing 100190, China*

²*University of Chinese Academy of Sciences, Beijing*

(Dated: July 9, 2018)

Tensor renormalization group method (TRG) is a real space renormalization group approach. It has been successfully applied to both classical and quantum systems. In this paper, we study a disordered and frustrated system, the two-dimensional Edward-Anderson model, by a new topological invariant TRG scheme. We propose an approach to calculate the local magnetizations and nearest pair correlations simultaneously. The Nishimori multi-critical point predicted by the topological invariant TRG agrees well with the recent Monte-Carlo results. The TRG schemes outperform the mean field methods on the calculation of the partition function. We notice that it maybe obtain a negative partition function at sufficiently low temperatures. However, the negative contribution can be neglected if the systems is large enough. This topological invariant TRG can also be used to study three-dimensional spin glass systems.

PACS numbers: 75.10.Nr, 05.10.Cc, 64.60.De

Keywords: Edward-Anderson model, spin glasses, tensor renormalization group

I. INTRODUCTION

Exploring the Edwards-Anderson (EA) model¹ is significant but extremely difficult. The nature of spin glasses on three-dimension is still a heat debate between the mean field picture and droplet picture²⁻⁷. over the past 30 years. For the two-dimensional (2D) model, besides its interests in statistical physics, it has wild applications on image processing⁸, computer vision^{9,10}, which is usually referred to as the Markov random field¹¹ in the computer scientists community. In this paper, we propose a coarse-graining method for EA model on 2D square lattice and calculate local physical quantities simultaneously by the tensor renormalization group (TRG) method.

TRG is a real space renormalization group approach initially introduced by Levin and Nave¹² for classical ferromagnetic Ising spin systems on 2D regular lattices. This method is an extension of the density matrix renormalization group method for one-dimensional quantum systems¹³. The basic idea is to perform a coarse-graining process on a tensor network. Matrix low rank approximation is used to cut the degree of freedom of tensor indices up to a maximum value D through the singular value decomposition.

Shortly after the introduction of the initial TRG method, an improvement was made by Xiang and co-authors¹⁴, who proposed a backward iteration to calculate the environment tensor and improved the results by considering the effect of the environment. The TRG method has excellent performance on the classical ferromagnetic Ising model, the Potts model¹⁵ and the diluted ferromagnetic model^{16,17}, etc. It also becomes a crucial tool to handle 2D quantum systems¹⁸⁻²⁰. Very recently a further improvement, namely the topological invariant TRG method, was proposed in the papers^{21,22} to extend

the TRG to three-dimensional (3D) ferromagnetic Ising cases.

Unlike the ferromagnetic Ising model, the EA spin glasses model¹ is heterogeneous, disordered and frustrated. It is intrinsic hard. The problems of finding a ground state of the 2D EA model with external field and the general 3D EA model are proved to belong to NP-hard class²³, which is commonly believed that no algorithm can solve them within polynomial time. In the previous study, the mean field approximation²⁴⁻²⁸ and Monte Carlo Sampling²⁹, transfer matrix method³⁰, numerical exact algorithm for 2D without the external field^{23,31} are used to calculate local properties for individual finite size instances. These methods are combined with finite size scaling to investigate the thermodynamics limit properties. The duality relationship³²⁻³⁴ and real space renormalization methods³⁵ are also employed to study the phase diagram and universality. TRG can be exploited in both of two roles. It can be served as an approximate calculator of physics quantities for a single instance, and it may also be used as a new renormalization method to directly investigate critical phenomenon. We, here, focus on the former role. To our best knowledges, there is no work on applying TRG on spin glasses until now.

In this paper, we proposed two main approaches. Firstly, we show a new topological invariant coarse-graining scheme based on the work²¹. It avoids two problems when the method²¹ is directly applied on EA model: cutting extra freedom of indices and inverting singular matrices. In the ferromagnetic Ising model, these two problems don't exist. Secondly, we propose an approach to compute local physical quantities simultaneously. For example, all single-spin magnetizations can be calculated by a single sweep of coarse-graining procedure and backward procedure. These two approaches are also useful

for other heterogeneous systems. In the numerical calculation, TRG may get a negative value of the partition function at very low temperature, which is the major difference between the spin glasses model and other heterogeneous systems^{16,17}. We show that the contribution of the negative part is comparable to the error fluctuation for a large enough system, and therefore it can be neglected. In the high temperature region, TRG outperforms the mean field method, belief propagation and generalized belief propagation^{24–28}, while the mean field methods are failed in the lower temperature because of the convergence problems. The Nishimori multi-critical point^{32,36,37} is calculated by our TRG scheme. The results agree well with the recent Monte-Carlo results²⁹. We emphasize that the original TRG method¹² can also be directly applied to any heterogeneous systems, including EA model, similar to the works on diluted ferromagnetic model^{16,17}. The advantage of topological invariant scheme is that it can be extended to 3D cases^{21,22}.

The paper is arranged as follows. In the remainder of Section 1, we introduce the EA model and show how to convert it to a tensor network. In section 2, we demonstrate our topological invariant TRG procedure. In section 3, we show how to calculate local physical quantities by backward iteration. In section 4, we list some numerical results to test the validation of this method. In section 5, we discuss the further improvement and applications.

II. THE MODELS

A. The Edward-Anderson Model

We consider the classical 2D EA model on a periodic square lattice with discrete coupling constants. The system consists of N spins $\{\sigma_i\}$, M coupling constants $\{J_{ij}\}$ and N local external fields $\{h_i\}$. Each spin σ_i takes value from $\{+1, -1\}$. The overall spins state $\underline{\sigma} = (\sigma_1, \sigma_2, \dots, \sigma_N)$ is referred to as a configuration. The energy function is defined as

$$H(\underline{\sigma}) = - \sum_{(ij) \in E} J_{ij} \sigma_i \sigma_j - \sum_{i \in V} h_i \sigma_i, \quad (1)$$

where E and V denote the edge set and vertex set of the system, respectively.

For a single instance of the EA model, the coupling constants and local external fields are fixed according to predefined distributions. In this paper, the value of J_{ij} is randomly chosen from the binomial distribution $P(J_{ij}) = p\delta(J_{ij}, 1) + (1-p)\delta(J_{ij}, -1)$, where $\delta(x, y)$ is the Kronecker delta symbol, which is 1 if $x = y$, otherwise is 0. The model parameter $0.5 \leq p \leq 1$ alters the system ranging from the spin glass ($p = 0.5$) to the pure ferromagnetic system ($p = 1$). The configuration $\underline{\sigma}$ is supposed to follow the Gibbs-Boltzmann distribution:

$$p(\underline{\sigma}) = \frac{1}{Z} \exp[-\beta H(\underline{\sigma})],$$

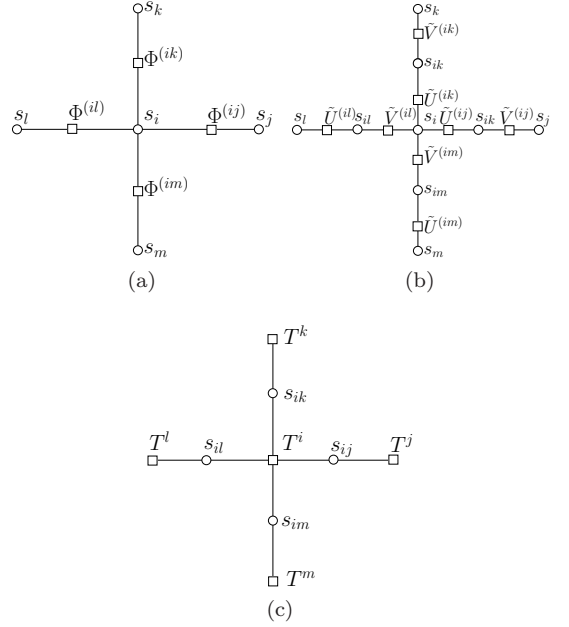


FIG. 1. Construction of a tensor network: (a) The neighborhood of a vertex i . (b) Each matrix $\phi^{(ij)}$ is split into two matrices by the singular value decomposition, so that each vertex i is now surrounded by four matrices which share the common index s_i . (c) Summing over the index s_i , the neighbor four matrices contract to be a tensor T^i .

where $Z = \sum_{\underline{\sigma}} \exp[-\beta H(\underline{\sigma})]$ is the partition function. It is useful to rewrite the distribution as a production of a set of non-negative weight factors

$$p(\underline{\sigma}) = \frac{1}{Z} \prod_{(ij) \in E} \psi_{ij}(\sigma_i, \sigma_j) \prod_{i \in V} \psi_i(\sigma_i), \quad (2)$$

where the weight factors have the form $\psi_{ij}(\sigma_i, \sigma_j) = \exp[\beta J_{ij} \sigma_i \sigma_j]$, $\psi_i(\sigma_i) = \exp[\beta h_i \sigma_i]$. If all the external random fields are zero, the partition function and the pair-spin correlations can be calculated exactly in polynomial time^{23,31,38}. However, for general external fields $\{h_i\}$, the problem is proved to be in the NP-hard class²³.

B. Tensor Networks

Any two-body interaction system can be transformed into a tensor network, in which the partition function of the system is equal to the trace of all the tensors. The transformation is not unique. Here we show a symmetric method. The transformation of the EA model on 2D square lattice at a site i is illustrated in Fig. 1. Firstly each Ising spin σ_i is mapped to a Boolean variable $s_i = (1 - \sigma_i)/2 \in \{0, 1\}$, so that each weight factor $\psi_{ij}(\sigma_i, \sigma_j)$ can be expressed as a matrix $\Phi^{(ij)}$, where the element in s_i -th row and s_j -th column is $\Phi_{s_i s_j}^{(ij)} = \psi_{ij}(1 - 2s_i, 1 - 2s_j)$. Note that the C-programming-language convention

is used, in which the index starts from 0. Meanwhile, each external weight factor $\psi_i(\sigma_i)$ of field h_i is mapped to a vector $\Phi^{(i)}$, of which the s_i -th element is $\Phi_{s_i}^{(i)} = \psi_i(1 - 2s_i)$. Next step, we perform the singular value decomposition on the matrix $\Phi^{(ij)}$, such that

$$\Phi_{s_i s_j}^{(ij)} = \sum_{s_{ij}} U_{s_i s_{ij}}^{(ij)} d_{s_{ij}} V_{s_j s_{ij}}^{(ij)}, \quad (3)$$

where the matrices $U^{(ij)}$, $V^{(ij)}$ are real orthogonal matrices and the vector $\underline{d} = (d_0, d_1)$ stores singular values in descending order. Each element in the vector \underline{d} is non-negative. The new variable $s_{ij} \in \{0, 1\}$ is the index of the singular vector \underline{d} . Let $\tilde{U}_{s_i s_{ij}}^{(ij)} = U_{s_i s_{ij}}^{(ij)} d_{s_{ij}}^{\frac{1}{2}}$, $\tilde{V}_{s_j s_{ij}}^{(ij)} = V_{s_j s_{ij}}^{(ij)} d_{s_{ij}}^{\frac{1}{2}}$. Then we have

$$\Phi_{s_i s_j}^{(ij)} = \sum_{s_{ij}} \tilde{U}_{s_i s_{ij}}^{(ij)} \tilde{V}_{s_j s_{ij}}^{(ij)}.$$

Now, each variable i is surrounded by four matrices $\tilde{U}_{s_i s_{ij}}^{(ij)}$, $\tilde{U}_{s_i s_{ik}}^{(ik)}$, $\tilde{V}_{s_i s_{il}}^{(il)}$, $\tilde{V}_{s_i s_{im}}^{(im)}$, where j, k, l, m are labels of the neighbor spins of the spin i . Finally, we sum over s_i and get a tensor $T_{s_{ij} s_{ik} s_{il} s_{im}}^i$:

$$T_{s_{ij} s_{ik} s_{il} s_{im}}^i = \sum_{s_i} \tilde{U}_{s_i s_{ij}}^{(ij)} \tilde{U}_{s_i s_{ik}}^{(ik)} \tilde{V}_{s_i s_{il}}^{(il)} \tilde{V}_{s_i s_{im}}^{(im)} \Phi_{s_i}^{(i)}. \quad (4)$$

The partition function of the original system is equal to the result obtained by tracing over all the indices of the tensors defined on lattice sites:

$$Z = \sum_{\{\underline{s}\}} \prod_i T_{s_{ij} s_{ik} s_{il} s_{im}}^i. \quad (5)$$

We refer to the network of tensors constructed by the above procedure as a tensor network. On the original lattice, each vertex i is associated with a tensor T^i , and each edge (ij) is associated with a tensor index s_{ij} . In graphical language, the tensor network is similar to a factor graph model with weight factors defined on vertices and state variables defined on edges, but a key difference is that the elements of tensors are not necessarily non-negative. In the following discussions, we rewrite the tensor indices as i_0, i_1, i_2, i_3 , i.e., $T_{i_0 i_1 i_2 i_3}^i$ for notational simplicity.

III. TENSOR COARSE-GRAINING PROCEDURE

There are several ways to implement the tensor coarse-graining procedure^{12,21,22}. Generally, each coarse-graining iteration consists of two steps. First is contracting two neighbor tensors into a new tensor with bigger indices freedom degree. It is an exact procedure. If there is no computation limitation, the exact partition function

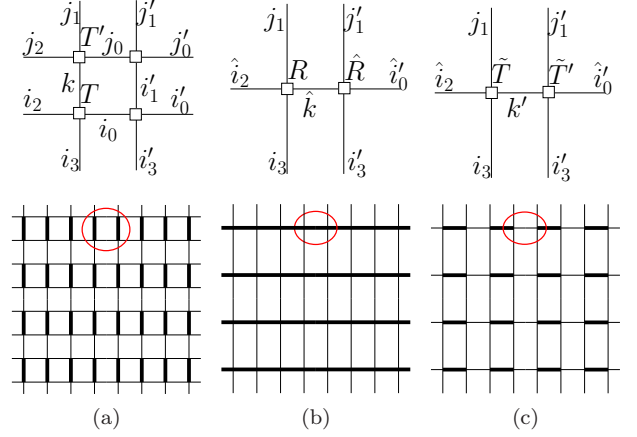


FIG. 2. (Color online) Demonstration of TRG: The top figure is the microscope of the circled region in the bottom figure. The two vertical tensors T and T' in (a) are contracted into one tensor R in (b), and the associated two indices i_0 and j_0 of (a) are combined into one index \hat{i}_0 . If the degree of freedoms of the index \hat{i}_0 is larger than the cut-off parameter D , we use the singular value decomposition to truncate this index and obtain the approximate tensors \tilde{T} and \tilde{T}' in (c). Bold lines indicates the freedom of associated indices are greater then the others, when the freedom exceeds the cut-off parameter D .

could be got by the iteration of these contractions. Second is cutting the indices freedom degree approximately, so that the computation is tractable.

We introduce our method for the tensor network defined on a 2D square lattice with the periodic boundary condition expressed as Eq. (5). At the first step, each two vertical neighbor-tensor pair T , T' are contracted as showed in Fig. 2a. We sum over the common index k , and the pair T , T' is unified into one tensor R :

$$R_{(i_0, j_0), j_1, (i_2, j_2), i_3} = \sum_k T_{i_0, k, i_2, i_3} T'_{j_0, j_1, j_2, k}. \quad (6)$$

The new tensor R has 6 indices $i_0, i_2, i_3, j_0, j_1, j_2$. We combine two indices in the same direction i_0, j_0 as a union index \hat{i}_0 and i_2, j_2 as another union index \hat{i}_2 , so that the number of indices of R is still 4, i.e., $\hat{i}_0, j_1, \hat{i}_2, i_3$. After the contraction, the topological structure of the square lattice is preserved, and the y-direction length shrinks to half, while the degrees of indices freedoms associated with the edges along the x-direction increases to the square of the previous one.

At the second step, the union indices \hat{i}_0 and \hat{i}_2 will be truncated alternatively along x-direction if their freedom degrees are greater then a given cut-off parameter D . Specifically, let us consider the two horizontal neighbor tensors $R_{\hat{k}, j_1, \hat{i}_2, i_3}$ and $R'_{i_0, j_1', \hat{k}, i_3}$ in Fig. 2b, which share a same index \hat{k} . We think R and R' as a sub-system in the tensor network with the internal variable \hat{k} and the boundary variables $\{\hat{k}, j_1, \hat{i}_2, i_3\}$ and $\{i_0, j_1', \hat{k}, i_3\}$. The boundary variables interact with other tensors, which can

be considered as the environment of the sub-system. We are going to approximate the sub-system by another one with a fewer freedom degree of internal variable such that the interaction with environment is as similar as possible. Mathematically, it is done by the lower rank matrix approximation. We rearrange the indices order of the tensor R as $j_1, \hat{i}_2, i_3, \hat{k}$, and group the first three indices as an unique index $\underline{i} = (j_1, \hat{i}_2, i_3)$. Then tensor R becomes a matrix $R_{\underline{i}, \hat{k}}$. In the same way, we get the matrix $R'_{\hat{k}, \underline{i}'}$ from the tensor R' , where $\underline{i}' = (\hat{i}'_0, j'_1, i'_3)$. We sum over the common index \hat{k} to get a new matrix A :

$$A_{\underline{i}, \underline{i}'} = \sum_{\hat{k}} R_{\underline{i}, \hat{k}} R'_{\hat{k}, \underline{i}'} . \quad (7)$$

The sub-system is now expressed by the matrix A . To exactly represent the boundary interaction, the minimum freedom degree of the internal variable is the rank of A . A lower rank approximation is made by the singular value decomposition. The matrix A is decomposed in the reduced form by

$$A_{\underline{i}, \underline{i}'} = \sum_{k'=0}^{\text{rank}(A)-1} U_{\underline{i}, k'} d_{k'} V_{\underline{i}', k'} . \quad (8)$$

The reduced singular value decomposition discards the zero elements of the singular vector d , which has no contribution to the sub-system. In the numerical computation, singular values less than the criterion $d_i < \epsilon = 10^{-12}$ are considered to be zero. If the rank of A is greater than the cut-off parameter D , we only keep the largest D singular values. Let $a' = \min\{\text{rank}(A), D\}$. The approximation of A is expressed as

$$A_{\underline{i}, \underline{i}'} \approx \tilde{A}_{\underline{i}, \underline{i}'} = \sum_{k'=0}^{a'-1} \tilde{T}_{\underline{i}, k'} \tilde{T}'_{k', \underline{i}'} , \quad (9)$$

where $\tilde{T}_{\underline{i}, k'} = U_{\underline{i}, k'} d_{k'}^{\frac{1}{2}}$ and $\tilde{T}'_{k', \underline{i}'} = V_{\underline{i}', k'} d_{k'}^{\frac{1}{2}}$. The matrices \tilde{T} and \tilde{T}' are non-singular, and therefore their inverse matrices always exists. This property will be used in the next section. Next, we expand the grouped indices \underline{i} and \underline{i}' and rearrange the order of indices to recover the tensor $\tilde{T}_{\hat{k}, j_1, \hat{i}_2, i_3}$ and $\tilde{T}'_{\hat{i}'_0, j'_1, \hat{k}, i'_3}$.

By this way, the tensors R and R' in Fig. 2b are replaced by \tilde{T} and \tilde{T}' in Fig. 2c, and the common index \hat{k} is replaced by k' whose degree of freedom is no greater than D . The above procedure of cutting off variable \hat{k} by the singular value decomposition guarantees that the matrix \tilde{A} is a best approximation of A among all matrices with the rank no greater than D , if the measure of the error is the Frobenius norm $\|A - \tilde{A}\|_F$. Note that A is a $D^6 \times D^6$ matrix. The complexity of directly decomposition of A is $O(D^{18})$. Considering that the rank of A is at most D^2 , we could reduce the complexity into $O(D^8)$. Details are illustrated in the appendix A.

We now rotate the present tensor network 90° in Fig. 2c, and then it has the same local structure of the tensor network as the one at the first step in Fig. 2a, while the length along x direction is reduced by half. We repeat the step 1 and step 2 once more. The size of the tensor network shrinks half both in x and y directions.

This is the complete step of a coarse-graining procedure. We repeat it, until the tensor network is reduced small enough to be tractable by brute-force summation to get the partition function. In this paper, the final size is 2×2 .

In practical, the value of elements of the tensors increase exponentially during the TRG procedure. So we need scale the tensor after each step. The scaling is forcing the maximum singular value of each $\tilde{A}^{(i)}$ in Eq. (9) in the present layer tensor network to be a fixed value S_m , and we save the logarithm of the scale factor for the i 'th matrix at the l 'th step as

$$\phi_l^{(i)} = \ln(d_0^{(i)}) - \ln(S_m), \quad (10)$$

where $d_0^{(i)}$ is the maximum singular value of matrix $\tilde{A}^{(i)}$. The total free energy density is

$$f(\beta) = -\frac{1}{N\beta} \left(\sum_l \sum_i \phi_l^{(i)} + \log Z_r \right), \quad (11)$$

where Z_r is the remaining scaled partition function calculated by contracting the final 2×2 tensor network.

The cut-off parameter D controls the space of approximate tensors when performing the coarse-graining procedure. If D is infinite large, the coarse-graining process is exact. Generally larger D will get more accurate results. In terms of computational complexity, our topological invariant TRG scheme is of order $O(D^8)$, while the original method¹² and the higher order TRG²¹ are $O(D^6)$ and $O(D^7)$, respectively. Practically, the precision in calculating the free energy is better than the original one¹² for the same cut-off parameter D . Our tensor coarse-graining method is based on the higher order TRG²¹, where the exact contraction step is same, but the approximate truncation is different. The higher order TRG method truncates all the indices associated with x-direction edges by the higher order singular value decomposition. However, we found that such a truncation scheme can't report a sufficiently precise free energy density value for the EA spin glass model. We only truncate the x-direction indices alternatively, while the remaining half of the x-direction indices will be contracted in the next step, so they are not necessary to be truncated.

IV. MARGINAL PROBABILITY AND BACKWARD PROCEDURE

The EA model has no translational symmetry, and therefore the local magnetization depends on vertex position. The marginal probability distribution of a vertex

i is given by:

$$P_i(s_i) = \frac{1}{Z} \sum_{\text{all indices}} T^i(s_i) \prod_{j \in V \setminus \{i\}} T^j, \quad (12)$$

where s_i is related to the spin σ_i by $\sigma_i = 1 - 2s_i$ and the term, all indices, under the summation is referred to as all the indices of every tensor in the tensor network $\{T^i | i \in V\}$, and $T^i(s_i)$ is a tensor at vertex i when its spin σ_i is fixed to $1 - 2s_i$:

$$T_{i_0 i_1 i_2 i_3}^i(s_i) = \tilde{U}_{s_i i_0} \tilde{U}'_{s_i i_2} \tilde{V}_{s_i i_3} \tilde{V}'_{s_i i_1} \Phi_{s_i}^{(i)}. \quad (13)$$

As showed in Eq. (12), $P_i(s_i)$ can be computed by ordinary TRG method for any i in the tensor network with a special tensor $T^i(s_i)$. However, it is impractical to calculate the marginal probabilities for all the vertices in this way. In this work we use the backward iteration method¹⁴ to compute the marginal spin probability distribution functions for all the vertices simultaneously.

We define the environment tensor, or just called the environment, of a local tensor T^i as

$$M_{i_0 i_1 i_2 i_3}^i = \sum_{\substack{\text{all indices} \\ \text{except } i_0, i_1, i_2, i_3}} \prod_{j \in V \setminus i} T^j, \quad (14)$$

where the summation is taken over all the indices of the tensor network except the indices of the tensor T^i . An environment M^i has the same indices as its correspondent tensor T^i . The partition function can be re-written as

$$Z = \sum_{i_0 i_1 i_2 i_3} T_{i_0 i_1 i_2 i_3}^i M_{i_0 i_1 i_2 i_3}^i. \quad (15)$$

And the marginal probability distribution is expressed as

$$P_i(s_i) = \frac{1}{Z} \sum_{i_0 i_1 i_2 i_3} T_{i_0 i_1 i_2 i_3}^i(s_i) M_{i_0 i_1 i_2 i_3}^i. \quad (16)$$

Similarly, the nearest-neighbor pair-wise marginal distribution $P_{ij}(s_i, s_j)$ can be also expressed as a summation between a pair of neighbor tensors and the correspond environment:

$$P_{ij}(s_i, s_j) = \frac{1}{Z} \sum_{i_0 j_0 j_1 i_2 j_2 i_3 k} T_{i_0 k i_2 i_3}^i(s_i) T_{j_0 j_1 j_2 k}^j(s_j) \times \hat{M}_{(i_0, j_0), j_1, (i_2, j_2), i_3}^{ij}, \quad (17)$$

where $\hat{M}_{(i_0, j_0), j_1, (i_2, j_2), i_3}^{ij}$ is the environment of the tensor $R_{(i_0, j_0), j_1, (i_2, j_2), i_3} = \sum_k T_{i_0 k i_2 i_3}^i T_{j_0 j_1 j_2 k}^j$.

We calculate environments of a tensor network at a more detailed level based on knowing the environments at a coarse-grained level, which we called the backward iteration. We start from the final coarse-grained 2×2 tensor network after finishing the forward TRG procedure. The corresponding environment M^i of a tensor T^i at this level can be calculated directly by tracing the other three tensors.

Given the environments $M^{\tilde{T}}, M^{\tilde{T}'}$ of the tensors \tilde{T}, \tilde{T}' in Fig. 2c, we now show how to calculate the environments $M^T, M^{T'}$ of the tensors T, T' at the detailed level in Fig. 2a. The definition of indices is the same as described in the previous section and shown in Fig. 2. We start from the relation equation of the tensor \tilde{T} and its environment $M^{\tilde{T}}$ in Eq. (15)

$$Z = \sum_{k', j_1, \hat{i}_2, i_3} \tilde{T}_{k', j_1, \hat{i}_2, i_3} M_{k', j_1, \hat{i}_2, i_3}^{\tilde{T}} \quad (18)$$

$$= \sum_{k', k'', \hat{i}} \tilde{T}_{k', \hat{i}} \delta_{k'', \hat{i}}^{k'} M_{k'', \hat{i}}, \quad (19)$$

where in the second line we group the indices (j_1, \hat{i}_2, i_3) as \hat{i} , and insert a Kronecker delta function $\delta_{k'', \hat{i}}^{k'}$.

The tensor $\tilde{T}'_{i'_0, j'_1, k', i'_3}$ can be viewed as a matrix $\tilde{T}'_{k', \hat{i}'}$ if we exchange the order of indices to $k', \hat{i}'_0, j'_1, i'_3$ and group the indices \hat{i}'_0, j'_1, i'_3 as \hat{i}' . As mentioned in previous section, the matrix $\tilde{T}'_{k', \hat{i}'}$ is always non-singular, we replace the Kronecker delta function in Eq. (19) by

$$\delta_{k'', \hat{i}'}^{k'} = \sum_{\hat{i}'} \tilde{T}'_{k', \hat{i}'} (\tilde{T}'^{-1})_{\hat{i}' k''}, \quad (20)$$

where \tilde{T}'^{-1} is the inverse of the matrix \tilde{T}' . The partition function is then expressed by

$$Z = \sum_{\hat{i}, \hat{j}} A_{\hat{i}, \hat{j}} M_{\hat{i}, \hat{j}}^{\tilde{A}}, \quad (21)$$

where $\tilde{A}_{\hat{i}, \hat{j}'} = \sum_{k'} \tilde{T}_{k', \hat{i}} \tilde{T}'_{k', \hat{j}'}$ is defined in Eq. (9), and $M^{\tilde{A}}$ is the environment of \tilde{A} :

$$M_{\hat{i}, \hat{j}'}^{\tilde{A}} = \sum_{k''} \left(\tilde{T}'^{-1} \right)_{\hat{j}', k''} M_{k'', \hat{i}} \quad (22)$$

Since \tilde{A} is the lower rank approximation of A , where $A_{\hat{i}, \hat{j}'} = \sum_{\hat{k}} R_{\hat{k}, \hat{i}} R'_{\hat{k}, \hat{j}'}$ defined in Eq. (7), the environment $M^{\tilde{A}}$ is approximately the environment of M^A

$$M^A \approx M^{\tilde{A}} \quad (23)$$

The physical explanation of the above approximation is that, for a sub-system expressed by \tilde{A} and its environment, if we replace this sub-system with another sub-system A , which interacts with the environment in a very similar way with more internal variable states, the environment will not change too much. From the relationship of A and its environment, we get

$$Z = \sum_{\hat{i}, \hat{i}', \hat{k}} R_{\hat{k}, \hat{i}} R'_{\hat{k}, \hat{i}'} M_{\hat{i}, \hat{i}'}^A.$$

The environments of R and R' are obtained as

$$M_{\hat{k}, \hat{i}}^R = \sum_{\hat{i}'} R'_{\hat{k}, \hat{i}'} M_{\hat{i}, \hat{i}'}^A, \quad (24)$$

$$M_{\hat{k}, \hat{i}'}^{R'} = \sum_{\hat{i}} R_{\hat{k}, \hat{i}} M_{\hat{i}, \hat{i}'}^A. \quad (25)$$

We expand the grouped indices $\underline{i}, \underline{i}'$ of matrices M^R and $M^{R'}$ and exchange the indices to get the environments $M_{\hat{k}, j_1, \hat{i}_2, i_3}^R$ and $M_{\hat{i}'_0, j'_1, \hat{k}, \hat{i}'_3}^{R'}$ of tensors R and R' . This is the backward iteration of the cut-off step.

The backward iteration of the contraction step is more straightforward. We unpack the indices \hat{k} and \hat{i}_2 of R in the view before contraction, hence $R_{\hat{k}, j_1, \hat{i}_2, i_3} \rightarrow R_{(i_0, j_0), j_1, (i_2, j_2), i_3} = \sum_k T_{i_0, k, i_2, i_3} T'_{j_0, j_1, j_2, k}$ as shown in Eq. (6), in which the first index \hat{i}_0 is the index \hat{k} here. From the relation of the tensor R and its environment

$$Z = \sum_{i_0 j_0 j_1 i_2 j_2 i_3 k} T_{i_0, k, i_2, i_3} T'_{j_0, j_1, j_2, k} M_{(i_0, j_0), j_1, (i_2, j_2), i_3}^R,$$

we can get the environments of T and T' as

$$M_{i_0, k, i_2, i_3}^T = \sum_{j_1 j_2 j_3} T'_{j_0, j_1, j_2, k} M_{(i_0, j_0), j_1, (i_2, j_2), i_3}^R, \quad (26)$$

$$M_{j_0, j_1, j_2, k}^{T'} = \sum_{i_0 i_1 i_2} T_{i_0, k, i_2, i_3} M_{(i_0, j_0), j_1, (i_2, j_2), i_3}^R. \quad (27)$$

After the above two steps, the environment matrix $M^{\hat{T}}$ is calculated by knowing the environment matrix M of higher coarse-grained level tensor network. We repeat this process until the environment tensors of the original tensor network are obtained. Then the marginal probability distributions can be calculated from Eq. (16). In practice, we reduce the computational complexity by utilizing the fact that the matrix A is at most rank D^2 .

The backward iteration is initially introduced to design a better way to do tensor coarse-graining by minimizing the change of the whole system with the environments¹⁴ on the ferromagnetic Ising model. This improvement can also be applied to EA model in the same way. We here exploit the backward iteration to calculate local physical quantities simultaneously.

V. NUMERICAL RESULTS

We compared the partition function calculated by our topological invariant TRG with those obtained by the original TRG¹² and mean field approach, belief propagation and generalized belief propagation (GBP)^{24,27,28}, on the pure spin glass model without external fields, i.e. $p = 0.5$ and $h_i = 0$. The exact partition function is calculated by the algorithm²³. The paramagnetic solutions of BP and GBP^{27,28} is included, which is the mean field method under the Bethe-Peierls approximation³⁹ and Kikuchi approximation⁴⁰ respectively. We measure the average error of the logarithm partition function as

$$\epsilon_\phi = \frac{1}{N} \langle |\log(Z_{exact}) - \log(Z)| \rangle \quad (28)$$

over 64 instances with $L=64$ in Fig. 3 in the region $\beta = 1/T \in [0, 1.1]$. The results show that tensor renormalization approaches outperforms BP and GBP in several orders. For the same cut-off parameter $D = 8$, our

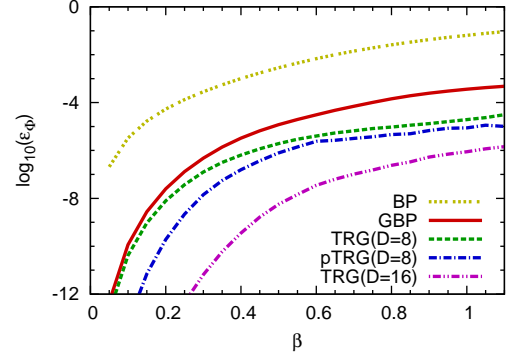


FIG. 3. (Color online) Comparison of the error of $\frac{1}{N} \log Z$, calculated by our topological invariant TRG (pTRG) with $D = 8$, the original TRG method (TRG)¹² with $D = 8, 16$, and the mean field approaches BP and GBP^{27,28}. The results are obtained by averaging, over 64 instances on a periodic square lattice with side length $L = 64$.

topological invariant TRG are more accurate than the original TRG. If one use a larger cut-off parameter D , the results will be better, while the computation time will increase dramatically.

At low temperatures T , i.e. high inverse temperature $\beta = 1/T$, we found that the TRG procedures may result in a negative partition function. This phenomenon happens both in the original TRG¹² and our topological invariant TRG. We tested 128 instances with the inverse temperature β ranging from 0 to 4.0. The probability of negative partition function is shown in Fig. 4a. A brief explanation is that the elements in the tensors do not constrained to be non-negative and the lower rank matrix approximation makes the final result to fluctuate around the exact partition function. At low temperatures, the error is so large that the scaled partition function Z_r of the final 2×2 tensor network turned out to be compatible with a negative value. It seems a general limitation of TRG methods applying for the models with frustrations. One could use larger cut-off parameter D to reduce the probability of negative results. If one only cares about the asymptotic result for a large system, one could simply neglect the negative part, since for infinite system the log partition function is dominated by the scaling factors $\Phi_l^{(i)}$ in each forward iteration step rather than the remaining contribution Z_r . To clarify this point, we define the ratio of remaining log partition function and the leading part of the scaling factors as r ,

$$r = \left\langle \frac{\log |Z_r|}{\sum_l \sum_i \Phi_l^{(i)}} \right\rangle, \quad (29)$$

where $\langle \cdot \rangle$ means averaging over disorders. Numerically, we averaged 128 instances. As showed in Fig. 4, the contribution of remaining free entropy decreases as the system size increase almost linearly in the log-log scale. For a large system, it will be even lower than the error, so that we can safely discard this term. This phenomenon

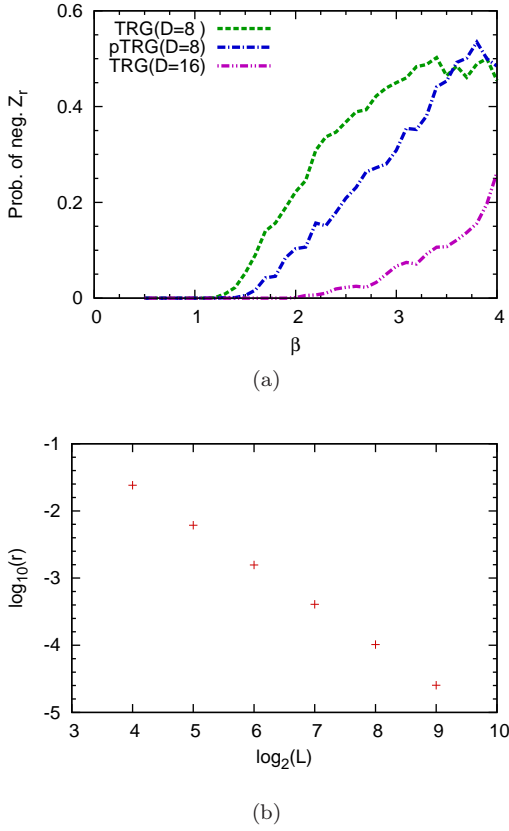


FIG. 4. (Color online) (a) The probability to obtain a negative Z_r and (b) The ratio r of $\log |Z_r|$ to the leading part at $\beta = 1.5$.

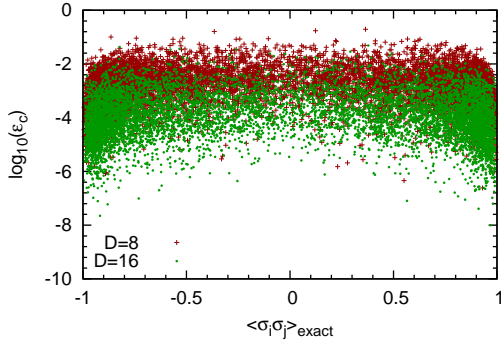


FIG. 5. (Color online) Comparing the nearest neighbor correlations of a single instance $L=64$ with exact results at $\beta = 1$. The cut-off parameter is set to $D = 8$ and 16 .

also indicates that we can investigate the EA model in the thermodynamic limit, similar to the work on ferromagnetic Ising model¹⁵. Because of the heterogeneity, the properties of the system are captured by infinite iterations of population of tensors rather than single tensor iteration. We leave the analysis of infinite systems in our future work.

We plot all the nearest-pair-spin correlations of a typi-

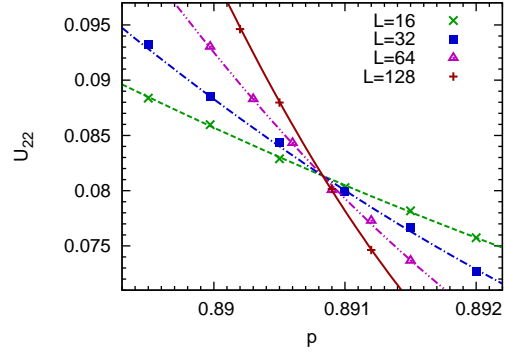


FIG. 6. (Color online) Estimation MNP point by finite size scaling. Lines are got by fitting Eq. (33).

cal single instance compared by the numerical exact values which are calculated by numerical differential of the free energy at $\beta = 1.0$. The error is defined by

$$\epsilon_c = (|\langle \sigma_i \sigma_j \rangle_{\text{pTRG}} - \langle \sigma_i \sigma_j \rangle_{\text{exact}}|) \quad (30)$$

Larger cut-off parameter D will lead to better results, as shown in Fig. 5. We do not show the local magnetizations since they are always zero because of the spin symmetry in the absence of no external fields.

The p - T phase diagram of 2D EA model has been extensively investigated in the papers^{29-37,41,42} and the references therein. There is no spin-glass phase occurred at finite temperature⁴², while it undergo a para-ferro magnetic phase transition at low temperature T and large p . The system is in the paramagnetic phase when $0.5 \leq p < p_c(T)$, and in the ferromagnetic phase when $p_c(T) < p \leq 1$. A special line $p_{\text{NL}}(T) = (\tanh(1/T) + 1)/2$ is called the Nishimori line³⁶, on which some physical quantities can be calculated exactly. The multi-critical Nishimori point (MNP) is the crossing point of the Nishimori line and the critical line $p_c(T)$. We compute the MNP by locating the crossing point.

We use the topological invariant TRG as a tool to calculate magnetizations, and compute susceptibility χ by numerical differential

$$\chi = \frac{d \sum_i \langle \sigma_i \rangle}{dh}, \quad (31)$$

where h is the external field and $\langle \cdot \rangle$ means averaging over the Boltzmann distribution, which can be quickly calculated by the marginal distribution Eq. (16) after the backward iteration. The MNP point is estimated by finite size scaling stated in the work²⁹. We measure the RG invariant quantity U_{22} , along Nishimori line near MNP, where

$$U_{22} = \frac{[\chi^2]}{[\chi]^2} - 1, \quad (32)$$

where the square brackets are referred to as the average over the disorder, i.e. the couplings $\{J_{ij}\}$. We use 2×10^5

TABLE I. Location of the multi-critical Nishimori point

Methods	p^*
BP ²⁸	0.79
GBP ^{27,28}	0.85
Duality Analysis ³²	0.889972
Duality Analysis ³³	0.890813
pTRG	0.890830(22)
Monte-Carlo ²⁹	0.89081(7)
Monte-Carlo ⁴³	0.89083(3)

instances for each point. Then, the MNP point is got by fitting

$$U_{22} = U_{22}^* + a_1(p - p^*)L^{y_1} + a_2(p - p^*)^2L^{2y_1}, \quad (33)$$

where U_{22}^* , a_n , p^* , y_1 are fitting parameters. We fit the data with the lattice size $16 \leq L \leq 128$ as showed in Fig. 6. and estimate the MNP point at $p^* = 0.890830 \pm 0.00022$, the exponent $y_1 = 0.642 \pm 0.022$ and other parameters $U_{22} = 0.0813 \pm 0.0003$, $a_1 = -0.85 \pm 0.07$, $a_2 = 6.5 \pm 2.6$. The chi-square test reports a small ratio of chi-square to the degree of freedom $\chi^2/DOF = 7.2/17$, which show the fit model are good enough to describe the data. We also test the fit by using different data group, for example $L \geq 32$, and $L \leq 64$. All test are consistent with each other, except the data of $L = 8$, which has strong finite size effect so that we discard it in all fit. The susceptibilities χ are checked by using different differential steps δh ranging from 10^{-6} to 10^{-3} . For most of instances, they are insensitive to δh , and we set $\delta h = 10^{-5}$. While, a tiny fraction (about 10^{-4}) depends on δh , and for these cases a larger δh is used. The location of MNP is not depend on the choices of δh . Small portions of instances are also verified by averaging the two-point correlations. The comparison of the estimation MNP is showed in Table I. The results agree well with the recent Monte Carlo method with finite size scaling²⁹, and the recent duality analysis inspired by hierarchical lattice³³. We leave the discussion of re-entrance phenomena and strong disorder universality as the future work. We emphasis that the role of TRG here is a new tool to calculate physical quantities. Compared other methods, the mean field estimation by BP and GBP on 2D EA model^{27,28}, it improve quite lot.

VI. DISCUSSIONS AND CONCLUSION

In this paper, we applied the TRG on the 2D EA model, and proposed a novel topological invariant tensor coarse-graining procedure, as well as an approach to calculate local physical quantities simultaneously. Two problems hidden in the translation symmetric cases are solved. We avoid to over-cut the freedom of indices in the coarse-graining procedure and avoid to inverse a singular matrix in backward iterations. The backward iteration process was used to compute single spin marginal

probability distributions and nearest neighbor spin pair correlations.

We found that the TRG scheme is able to compute the free energy and local correlations accurately if the temperature is not very low. At low temperatures the TRG scheme might lead to a negative value of the partition function. We show that, for large systems, the main contribution of the partition function is the scaling factors during the coarse-graining iteration, and the negative remaining scaled partition function of the final 2×2 tensor networks can be discarded. The successful estimation of the MNP location indicates TRG can be used in studying the critical phenomena in a satisfied precision¹⁵, though originally TRG is considered only be applied to gapped phase¹². The present TRG scheme can't be applied to the case at zero temperature, because the SVD only preserves local optimal coarse-graining mode, and they are orthogonal in the further coarse-graining iteration and finally get zero partition function. It's an open question that whether TRG can be used at zero temperature problem. A further improvement can be made by considering the effect of environments, which is illustrated in the paper^{14,21} on the ferromagnetic Ising model. In principle, one can investigate the fixed point of TRG. However, it may not get a good precision as we did in our paper, because the advantage of TRG is its excellence performance on compute physical quantities rather than analyzing the fix point of the renormalization⁴⁴.

The topic on the nature of spin glass phase on 3D lattice is still rather active²⁻⁷. The main method in most of the current studies is the Monte-Carlo Sampling. The topological invariant coarse-graining iteration can be done in 3D cases by contracting tensors along one direction, and cut off the indices associated to the edges along the other two directions. Local physical quantities, for example the Edward-Anderson parameter, can be directly got as showed in this paper. The sample-to-sample overlap distribution or other non-local quantities would be estimated by TRG guided sampling, in the way that we fix the spins one by one according to its marginal probability. So, it presents an alternative way to investigate 3D spin glass models.

Another application is on investigating combinatorial optimization problems on finite-dimensional lattices or loopy random graphs. TRG can be immediately applied on image segmentation and denoising⁸. They share the same mathematical structure as 2D spin glasses model. For random graph model, mean field method provided excellent solutions on mean-field like systems, such as local-tree like structured graph⁴⁵ and fully connected graph⁴⁶. While, for the system rich in local loops, the mean field approximate may not quite accurate, for example small world networks, and many real networks. The extension of TRG on general graph provides a new insight and maybe another physics-contributed solution to such problems. Similar to the belief propagation, the decimation⁴⁷ and reinforcement approaches⁴⁸ can be combined with TRG to get optimization solutions.

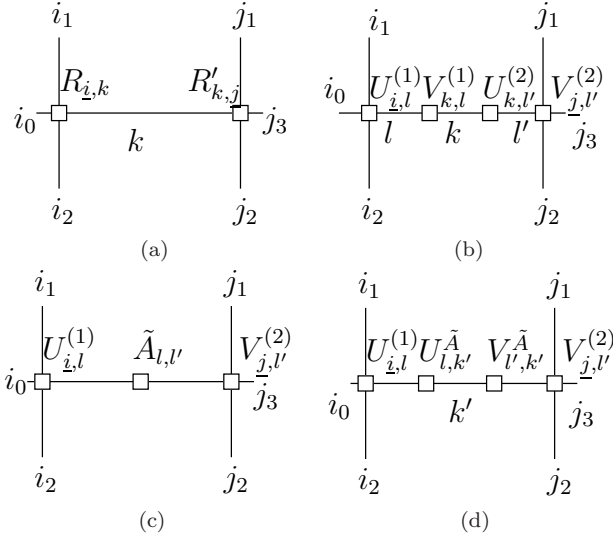


FIG. 7. Demonstration of simplifying cut-off step

ACKNOWLEDGMENTS

We thank Qiao-Ni Chen, Zhi-Yuan Xie, Jin-Fang Fan, Jack Raymond, Victor Martin-Mayor for helpful discussions, and thank Jack Raymond for comments on an earlier version of the manuscript. H.-J. Zhou were supported by the National Basic Research Program of China (No. 2013CB932804), the Knowledge Innovation Program of Chinese Academy of Sciences (No. KJCX2-EW-J02), and the National Science Foundation of China (grant Nos. 11121403, 11225526). The numerical simulations were performed in the HPC computer cluster of ITP-CAS and we thank Dr. Hongbo Jin for technical helps.

Appendix A: Simplifying Singular Value Decomposition of Matrix A

We started from the definition of the matrix A in Eq. (7), where R and R' are tensors with four indices. We exchange and combine the indices so that $R_{\hat{k},j_1,\hat{i}_2,i_3}$, $R'_{\hat{i}'_0,j'_1,\hat{k},i'_3}$ change to be matrices $\hat{R}_{(j_1,\hat{i}_2,i_3);\hat{k}}$, $\hat{R}'_{(\hat{i}'_0,j'_1,i'_3);\hat{k}}$. For simplicity we write $\underline{i} = (j_1, \hat{i}_2, i_3)$, and $\underline{i}' = (\hat{i}'_0, j'_1, i'_3)$. Instead of multiplying R and R' , here we firstly decompose them by the singular value decomposition

$$R_{\underline{i},k} = \sum_l U_{\underline{i},l} d_l V_{l,k}, \quad (A1)$$

$$R'_{k,\underline{i}'} = \sum_{l'} U'_{k,l'} d_{l'} V'_{l',\underline{i}'}. \quad (A2)$$

Let

$$\tilde{A}_{l,l'} = \sum_k d_l V_{l,k} U'_{k,l'} d_{l'}. \quad (A3)$$

We decompose \tilde{A} by the singular value decomposition

$$\tilde{A}_{l,l'} = \sum_{k'} U^A_{l,k'} d^A_{k'} V^A_{l',k'}. \quad (A4)$$

Then tensors $\tilde{T}_{\underline{i},k'}$, $\tilde{T}'_{\underline{j},k'}$ in Eq (9), could be calculated by

$$\tilde{T}_{\underline{i},k'} = \sum_l U_{\underline{i},l} U^A_{l,k'} d_l^{A\frac{1}{2}}, \quad (A5)$$

$$\tilde{T}'_{\underline{j},k'} = \sum_{l'} d_l^{A\frac{1}{2}} V^A_{l',k'} V'_{l',\underline{j}}. \quad (A6)$$

The numerical SVD routines takes $O(mn^2)$ flops to decompose a $m \times n$ matrix ($m \geq n$) by Golub-Reinsch algorithm⁴⁹. The SVD routine in GNU Scientific Library is used in our numerical calculation. The maximum size of matrix \hat{R} , and \hat{R}' are $D^4 \times D$. The SVD of these two matrices takes $O(D^8)$ flops, which take most computational complexity in the coarse-graining step, while directly decomposing the $D^6 \times D^6$ matrix A in Eq. (8) takes $O(D^{18})$ flops.

* wangchuang@itp.ac.cn

¹ S. F. Edwards and P. W. Anderson, J. Phys. F Met. Phys. **5**, 965 (1975).

² G. Parisi, Phys. Rev. Lett. **50**, 1946 (1983).

³ D. S. Fisher and D. A. Huse, Phys. Rev. B **38**, 386 (1988).

⁴ B. Yucesoy, H. G. Katzgraber, and J. Machta, Phys. Rev. Lett. **109**, 177204 (2012).

⁵ A. Billoire, L. A. Fernandez, A. Maiorano, E. Marinari, V. Martin-Mayor, G. Parisi, F. Ricci-Tersenghi, J. J. Ruiz-Lorenzo, and D. Yllanes, Phys. Rev. Lett. **110**, 219701 (2013).

⁶ C. K. Thomas, D. A. Huse, and A. A. Middleton, Phys.

Rev. Lett. **107**, 047203 (2011).

⁷ F. Parisen Toldin, A. Pelissetto, and E. Vicari, Phys. Rev. E **84**, 051116 (2011).

⁸ K. Tanaka, J.-i. Inoue, and D. Titterton, J. Phys. A **36**, 11023 (2003).

⁹ H. Derin and H. Elliott, IEEE Trans. Pattern Anal. Machine Intell. , 39 (1987).

¹⁰ J. Sun, N.-N. Zheng, and H.-Y. Shum, IEEE Trans. Pattern Anal. Mach. Intell. **25**, 787 (2003).

¹¹ S. Z. Li, in *Computer Vision ECCV'94* (Springer, 1994) pp. 361–370.

¹² M. Levin and C. P. Nave, Phys. Rev. Lett. **99**, 120601

- (2007).
- ¹³ U. Schollwöck, *Rev. Mod. Phys.* **77**, 259 (2005).
 - ¹⁴ Z.-Y. Xie, H.-C. Jiang, Q.-N. Chen, Z.-Y. Weng, and T. Xiang, *Phys. Rev. Lett.* **103**, 160601 (2009).
 - ¹⁵ M. Hinczewski and A. N. Berker, *Phys. Rev. E* **77**, 011104 (2008).
 - ¹⁶ C. Güven, M. Hinczewski, and A. N. Berker, *Phys. Rev. E* **82**, 051110 (2010).
 - ¹⁷ C. Güven and M. Hinczewski, *Phys. A* **389**, 2915 (2010).
 - ¹⁸ H.-C. Jiang, Z.-Y. Weng, and T. Xiang, *Phys. Rev. Lett.* **101**, 090603 (2008).
 - ¹⁹ Z.-C. Gu, M. Levin, and X.-G. Wen, *Phys. Rev. B* **78**, 205116 (2008).
 - ²⁰ W. Li, S.-J. Ran, S.-S. Gong, Y. Zhao, B. Xi, F. Ye, and G. Su, *Phys. Rev. Lett.* **106**, 127202 (2011).
 - ²¹ Z.-Y. Xie, J. Chen, M.-P. Qin, J.-W. Zhu, L.-P. Yang, and T. Xiang, *Phys. Rev. B* **86**, 045139 (2012).
 - ²² A. García-Sáez and J. I. Latorre, *Phys. Rev. B* **87**, 085130 (2013).
 - ²³ F. Barahona, *J. Phys. A*, 3241 (1982).
 - ²⁴ J. S. Yedidia, W. T. Freeman, and Y. Weiss, *IEEE Trans. Inf. Theory* **51**, 2282 (2005).
 - ²⁵ H.-J. Zhou, C. Wang, J.-Q. Xiao, and Z.-D. Bi, *J. Stat. Mech. Theor. Exp.* **2011**, L12001 (2011).
 - ²⁶ H.-J. Zhou and C. Wang, *J. Stat. Phys.* **148**, 513 (2012).
 - ²⁷ C. Wang and H.-J. Zhou, *JPCS* **473**, 012004 (2013).
 - ²⁸ A. Lage-Castellanos, R. Mulet, F. Ricci-Tersenghi, and T. Rizzo, *J. Phys. A* **46**, 135001 (2013).
 - ²⁹ M. Hasenbusch, F. Parisen Toldin, A. Pelissetto, and E. Vicari, *Phys. Rev. E* **77**, 051115 (2008).
 - ³⁰ Y. Ozeki and H. Nishimori, *J. Phys. Soc. Jpn.* **56**, 3265 (1987).
 - ³¹ C. K. Thomas and A. A. Middleton, *Phys. Rev. E* **87**, 043303 (2013).
 - ³² H. Nishimori and K. Nemoto, *J. Phys. Soc. Japan* **71**, 1198 (2002).
 - ³³ M. Ohzeki, *Phys. Rev. E* **79**, 021129 (2009).
 - ³⁴ M. Ohzeki, C. K. Thomas, H. G. Katzgraber, H. Bombin, and M. Martin-Delgado, *J. Stat. Mech. Theor. Exp.* **2011**, P02004 (2011).
 - ³⁵ T. Jörg and F. Krzakala, *J. Stat. Mech. Theor. Exp.* **2012**, L01001 (2012).
 - ³⁶ H. Nishimori, *Prog. Theor. Phys.* **66**, 1169 (1981).
 - ³⁷ K. Takeda, T. Sasamoto, and H. Nishimori, *J. Phys. A* **38**, 3751 (2005).
 - ³⁸ P. W. Kasteleyn, *Physica* **27**, 1209 (1961).
 - ³⁹ H. Bethe, *Proc. R. Soc. London. Ser. A*, 552 (1935).
 - ⁴⁰ R. Kikuchi, *Phys. Rev.* **81**, 988 (1951).
 - ⁴¹ F. D. Nobre, *Phys. Rev. E* **64**, 046108 (2001).
 - ⁴² R. N. Bhatt and A. P. Young, *Phys. Rev. B* **37**, 5606 (1988).
 - ⁴³ F. Parisen Toldin, A. Pelissetto, and E. Vicari, *J. Stat. Phys.* **135**, 1039 (2009).
 - ⁴⁴ E. Efrati, Z. Wang, A. Kolan, and L. P. Kadanoff, *Rev. Mod. Phys.* **86**, 647 (2014).
 - ⁴⁵ M. Mézard and G. Parisi, *Eur. Phys. J. B* **20**, 217 (2001).
 - ⁴⁶ D. Sherrington and S. Kirkpatrick, *Phys. Rev. Lett.* **35**, 1792 (1975).
 - ⁴⁷ M. Mézard and R. Zecchina, *Phys. Rev. E* **66**, 056126 (2002).
 - ⁴⁸ J. Chavas, C. Furtlehner, M. Mézard, and R. Zecchina, *J. Stat. Mech. Theor. Exp.* **2005**, P11016 (2005).
 - ⁴⁹ G. H. Golub and C. Reinsch, *Numerische Mathematik* **14**, 403 (1970).